Decomposition of electromagnetic fields into upgoing and downgoing components

Lasse Amundsen[1], Lars Løseth[2], Rune Mittet[3], Svein Ellingsrud[3], and Bjørn Ursin[4]

ABSTRACT

This paper gives a unified treatment of electromagnetic (EM) field decomposition into upgoing and downgoing components for conductive and nonconductive media, where the electromagnetic data are measured on a plane in which the electric permittivity, magnetic permeability, and electrical conductivity are known constants with respect to space and time. Above and below the plane of measurement, the medium can be arbitrarily inhomogeneous and anisotropic.

In particular, the proposed decomposition theory applies to marine EM, low-frequency data acquired for hydrocarbon mapping where the upgoing components of the recorded field guided and refracted from the reservoir, that are of interest for the interpretation. The direct-source field, the refracted airwave induced by the source, the reflected field from the sea surface, and most magnetotelluric noise traveling downward just below the seabed are field components that are considered to be noise in electromagnetic measurements.

The viability and validity of the decomposition method is demonstrated using modeled and real marine EM data, also termed seabed logging (SBL) data. The synthetic data are simulated in a model that is fairly representative of the geologic area where the real SBL were collected. The results from the synthetic data study therefore are used to assist in the interpretation of the real data from an area with 320-m water depth above a known gas province offshore Norway. The effect of the airwave is seen clearly in measured data. After field decomposition just below the seabed, the upgoing component of the recorded electric field has almost linear phase, indicating that most of the effect of the airwave component has been removed.

INTRODUCTION

Marine electromagnetic (EM) exploration is a new geophysical tool for locating offshore hydrocarbon reserves. EM seabed logging (EMSBL), illustrated in Figure 1, is essentially a marine EM data acquisition technique in which electric- and magnetic-field sensors on a grid or along a line are placed on the seafloor in and around a target area, and a powerful mobile horizontal electric dipole source transmits a low-frequency EM signal down through the underlying rock formations (Eidesmo et al., 2002; Ellingsrud et al., 2002). The principle of EMSBL is that it exploits the large resistivity contrast (known to exist from standard borehole logging) between oil or gas reservoirs and their surrounding water-filled sediments. In the presence of hydrocarbons, signals are guided and refracted back as upgoing modes to the seabed, where they are recorded.

Seabed logging (SBL) is a special application of controlled-source electromagnetic (CSEM) sounding (see, e.g., Young and Cox, 1981; Chave and Cox, 1982; and Sinha et al., 1990). CSEM sounding has been used successfully for a number of years to study ocean basins and active spreading centers. SBL is the first application of CSEM for remote and direct detection of hydrocarbons in the marine environment.

Figure 2 illustrates the principal upgoing and downgoing field components in the EMSBL survey. Even though the illustration
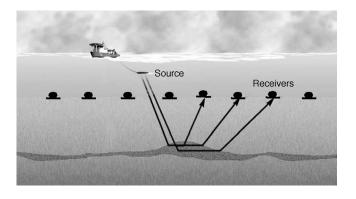
Figure 1. Principle of marine EMSBL for hydrocarbon mapping. The method exploits the large resistivity contrast between oil or gas reservoirs and their surrounding water-filled sediments. In the EMSBL experiment, sensors on a grid or along a line are placed on the seafloor in and around a target area, and a powerful source transmits a low-frequency EM signal down through the underlying rock formations. EM energy is rapidly attenuated in the conductive subsurface sediments because of water-filled pores. In high-resistance layers, such as hydrocarbon-filled sandstones, and at a critical angle of incidence, the energy is refracted and guided along the layers, and is attenuated to a lesser extent. This energy is refracted back to the seabed, where it is recorded. The detection, processing, and interpretation of guided and refracted energy is the basis of EMSBL.
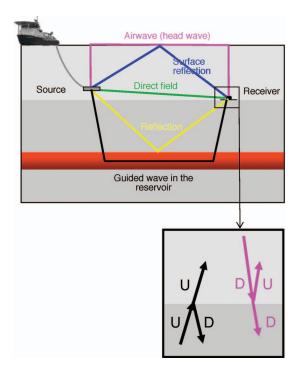

Figure 2. Simplified model used to illustrate some of the dominating field modes (events) in the EMSBL experiment. The EM energy that is generated by the source is spread in all directions — into the overlying water column, directly to the receiver, and downward into the seabed. Note that all fields traveling downward (D) in the water column also are downward-traveling fields just below the seabed, whereas they give rise to an upward (U) reflection just above the seabed. Therefore, it is desirable to perform the up/down field decomposition just below the seabed.

model is extremely simplified compared to any real geology above which SBL data are collected, it still conveys the main principles and data-processing challenges related to the SBL concept. The events of main interest for hydrocarbon mapping involve only a single reflection, a single refraction, or a guided event from the reservoir. These are detected as upgoing events by the sensors. A problem that arises in EMSBL is that EM energy may travel from the source to the receiver along many paths. The direct field is the signal that is transmitted directly from the source to the receiver. The direct field dominates in amplitude strength at short source/receiver separations, but it is strongly damped at larger offsets because seawater has high conductivity. In shallow water, EMSBL exploration also is complicated by other source-induced fields received at the receiver array as downward-traveling components that have been refracted and reflected off the sea surface. The airwave is dominated by the signal component that propagates upward from the source to the sea surface, horizontally through the air with no attenuation, and back down through the water column to the receiver. Because of the extreme velocity contrast between water and air, the critical angle for total reflection between seawater and air occurs at almost normal incidence. For angles of incidence greater than the critical angle, total reflection takes place, and the air volume acts as a perfect mirror for upgoing energy. The surface reflection has its geometrical reflection approximately midway between the source and the receiver. (The source is towed approximately 10 m above the seabed, while the receiver remains stationary on the seabed.) In terms of signal strength at the receiver, unless the water is deep, the sea-surface boundary is an efficient reflector at small to moderate offsets, and is an efficient refractor at larger offsets. The downward-traveling fields interfere with the upgoing fields from the subsurface. Reflections and refractions from the sea surface thus can be a severe problem, particularly in shallow-water EM exploration. If the sea surface reflections and refractions are not properly attenuated, they interfere with and overlap primary reflections and refractions from the subsurface. Optimal processing, analysis, and interpretation of EM data ideally require full information about the field, so that the field can be decomposed into its upgoing and downgoing constituents.

As Figure 2 illustrates, just below the seabed, the direct field from the source and the reflections and refractions from the sea surface always are downgoing modes; however, the reflections and refractions of interest from the subsurface are upgoing modes below the seabed. It therefore is desirable to separate, just below the seabed, the EM field measured at the seabed into its upgoing and downgoing components. In the special case that the change in medium parameters across the seabed is small, so that reflections and refractions at the seabed are insignificant in amplitude compared to signals from below, decomposition of the EM field just above the seafloor can be as effective as field decomposition just below the seafloor.

An additional benefit of field separation into upgoing and downgoing components is that magnetotelluric (MT) noise (Vozoff, 1986) in the downgoing component is attenuated. The upgoing component, which is of interest for interpretation, will be affected only by the reflected MT noise, which is much weaker than the direct MT field.

Our main objective is to provide a method for decomposing the EM field recorded along one or several receiver arrays into its upgoing and downgoing components. The technique can be used on marine EM data recorded on an areal grid, along a profile (line) (under specified assumptions), or at a single station receiver. Because of possible differences in transfer functions of the electric- and magnet-

ic-field sensors, each recorded component of the EM field must be properly calibrated before the decomposition technique is applied. This ensures that the calibrated components of the measured EM field fulfill Maxwell's equations as closely as possible.

We first write Maxwell's equations in the form of a matrix system of differential equations in the frequency-wavenumber domain. We assume that the EM field has been measured along a horizontal receiver plane where the medium is isotropic and homogeneous. Above and below the receiver plane, the medium can be arbitrarily inhomogeneous and anisotropic. The dependent field variables are the horizontal components of the electric and magnetic fields. Then, an eigenequation analysis allows us to locally decompose the EM field into upgoing and downgoing constituents. Finally, the decomposition technique is applied to synthetic and real SBL data.

The decomposition technique presented in this paper treats the EMSBL field as a wavefield. In Appendix A, we show to those with rusty skills in EM wave theory that the wave theory point of view gives a unified description of EM wave propagation in both conductive and nonconductive media. Some text books that treat EM-wave propagation in conductive materials are Morse and Feshbach (1953), Jackson (1999), Griffiths (1999), and Ulaby (2001). Also see Wait (1970), Chave and Cox (1982), Ward and Hohmann (1987), and Løseth et al. (2006). In treating the EMSBL field as a wavefield with a complex wavenumber, we fully account for the diffusion properties of the EMSBL field. Therefore, to achieve EM field decomposition, we can use all the well-established tools of wave theory that are developed in electrodynamics, and in elastodynamics. This is no surprise because it is well known that these two disciplines share a mathematical unity that is manifested in the vector Helmholtz equations that the time-harmonic fields obey. Thus, EM-field decomposition can be carried out very analogously to elastodynamic wavefield decomposition. As such, our approach for EM field decomposition follows the classic work of Ursin (1983) and Kennett (1983). The equivalent method for wavefield decomposition of four-component ocean-bottom seismic (4C-OBS) data was first presented by Amundsen and Reitan (1995).

PREVIOUS WORK ON EM-FIELD DECOMPOSITION INTO UPGOING AND DOWNGOING COMPONENTS

This section briefly reviews previous approaches for EM-field decomposition into upgoing and downgoing components.

In his review paper on 3D elastic- and electromagnetic-wave propagation in layered media, Ursin (1983) gave a unified treatment of elastic and electromagnetic wavefield decomposition in 1D media. Ursin (1983) scaled the amplitudes of the upgoing and downgoing waves with respect to the vertical energy flux. This yields symmetry properties that may be used in the analysis of reflection and transmission responses of a layered medium.

In developing an approach to construct a pseudoimpulse response for MT data, Levy et al. (1988) showed for 1D EM plane-wave propagation how the electric and magnetic components of the transverse-magnetic (TM) mode data could be converted to upgoing and downgoing waves. Zhdanov et al. (1996) presented a method for resistivity imaging based on frequency-domain migration of EM data obeying the diffusion equation. They suggest that, before the migration is carried out, the measurements of the electric and magnetic fields at the earth's surface be separated into upgoing and downgoing fields, similar to what can be done before seismic migration when the com-

plete wavefield is recorded. Zhdanov et al. (1996), who followed the Berdichevsky and Zhdanov (1984) approach of dividing the EM field into external and internal parts, gave their technique for field separation for a limited number of cases: transverse-electric (TE) polarization for 2D and 1D propagation of the E_2 component, and TM polarization for 1D propagation of the H_2 component.

EM-field decomposition also applies in principle to multicomponent ground-penetrating radar (GPR) data (see, e.g., van der Kruk, 2001).

In this paper, we extend the EM-field separation work of Ursin (1983), Levy et al. (1988), and Zhdanov et al. (1996) in the following way:

- The decomposition of the field obeying the 3D Maxwell's equations is treated in a unified manner for both conductive and nonconductive 3D media that can vary arbitrarily below the plane of measurement. The theory is valid for any type of conductive medium: good conductors, quasiconductors, and low-loss dielectrics.
- Contrary to Ursin (1983) we scale the amplitudes of the upgoing and downgoing components with respect to the field's amplitude.
- We list 2D and 1D field propagation as special cases.

MAXWELL'S EQUATIONS

We assume that the EM field has been measured along the horizontal receiver plane, where the material parameters of magnetic permeability μ, the electric permittivity ε, and the electric conductivity σ do not vary laterally and are time-invariant. Nonconductive media have extremely low values of σ, and are idealized as $\sigma = 0$. Thus, in the present work, nonconductive media can be seen as a special case of conductive media. Above and below the receivers, the medium can be arbitrarily inhomogeneous and anisotropic.

Let $\mathbf{x} = (x_1, x_2, x_3) = (x, y, z)$ denote a fixed coordinate system with the depth axis positive downward. Maxwell's equations for the electric and magnetic fields for an isotropic and source-free region can be given in the forms (Morse and Feshbach, 1953)

$$\nabla \times \hat{\mathbf{E}}(\mathbf{x}, t) = -\mu \partial_t \hat{\mathbf{H}}(\mathbf{x}, t) \quad (1)$$

and

$$\nabla \times \hat{\mathbf{H}}(\mathbf{x}, t) = (\sigma + \varepsilon \partial_t) \hat{\mathbf{E}}(\mathbf{x}, t), \quad (2)$$

where $\hat{\mathbf{E}} = (\hat{E}_1, \hat{E}_2, \hat{E}_3)^T$ is the electric field, $\hat{\mathbf{H}} = (\hat{H}_1, \hat{H}_2, \hat{H}_3)^T$ is the magnetic field, and the superscript T denotes transpose. We introduce the Fourier transform with respect to time and horizontal spatial coordinates,

$$G(k_1, k_2, \omega) = \int_{-\infty}^{\infty} \int_{-\infty}^{\infty} \int_{-\infty}^{\infty} dx_1 dx_2 dt$$

$$\times \exp[-i(k_1 x_1 + k_2 x_2 - \omega t)] \hat{G}(x_1, x_2, t), \quad (3)$$

with its inverse,

$$\hat{G}(x_1, x_2, t) = \frac{1}{(2\pi)^3} \int_{-\infty}^{\infty} \int_{-\infty}^{\infty} \int_{-\infty}^{\infty} dk_1 dk_2 d\omega$$

$$\times \exp[i(k_1 x_1 + k_2 x_2 - \omega t)] G(k_1, k_2, \omega), \quad (4)$$

where k_1 and k_2 are the horizontal wavenumbers conjugate to x_1 and

x_2, respectively, and where ω is the circular frequency. Applying the Fourier transform to Maxwell's equations 1 and 2, and algebraically eliminating E_3 and H_3 yield the ordinary matrix-vector differential equation (Ursin, 1983),

$$\partial_3 \mathbf{b} = i\omega \mathbf{A} \mathbf{b}, \tag{5}$$

where the electric-magnetic-field vector $\mathbf{b}$ is a 4×1 column vector,

$$\mathbf{b} = (\boldsymbol{\mathcal{E}}^T, \boldsymbol{\mathcal{H}}^T)^T, \tag{6}$$

and the electric $\boldsymbol{\mathcal{E}} = (E_1, E_2)^T$ and magnetic $\boldsymbol{\mathcal{H}} = (-H_2, H_1)^T$ field vectors are 2×1 column vectors. The 4×4 system matrix $\mathbf{A}$ is partitioned into four 2×2 submatrices, of which the diagonal ones are zero:

$$\mathbf{A} = \begin{bmatrix} \mathbf{0} & \mathbf{A}_1 \\ \mathbf{A}_2 & \mathbf{0} \end{bmatrix}. \tag{7}$$

The symmetric submatrices $\mathbf{A}_1$ and $\mathbf{A}_2$,

$$\mathbf{A}_1 = -\tilde{\varepsilon}^{-1} \begin{bmatrix} q_1^2 & -p_1 p_2 \\ -p_1 p_2 & q_2^2 \end{bmatrix},$$
$$\mathbf{A}_2 = -\mu^{-1} \begin{bmatrix} q_2^2 & p_1 p_2 \\ p_1 p_2 & q_1^2 \end{bmatrix}, \tag{8}$$

are functions of the parameters in Maxwell's equations and of the horizontal slowness components,

$$p_i = \frac{k_i}{\omega}, \quad i = 1, 2. \tag{9}$$

The vertical slowness is given by

$$q = \sqrt{\tilde{c}^{-2} - p^2}, \tag{10}$$

where $p^2 = p_1^2 + p_2^2$ and where

$$\tilde{c} = -\frac{1}{\sqrt{(\mu\tilde{\varepsilon})}} \tag{11}$$

is the complex velocity defined through the complex permittivity,

$$\tilde{\varepsilon} = \varepsilon\left(1 + \frac{i\sigma}{\omega\varepsilon}\right). \tag{12}$$

Two special cases of vertical slowness are

$$q_i = \sqrt{\tilde{c}^{-2} - p_i^2}, \quad i = 1, 2. \tag{13}$$

For notational convenience, the explicit dependence of different quantities on frequency, wavenumber, depth, etc., is omitted. For instance, the electric-field vector $\hat{\boldsymbol{\mathcal{E}}}(x_1, x_2, x_3, t)$, recorded at depth x_3, is in the wavenumber domain denoted by $\boldsymbol{\mathcal{E}}$, with the understanding that $\boldsymbol{\mathcal{E}} = \boldsymbol{\mathcal{E}}(k_1, k_2, x_3, \omega)$.

In equation 12, we combine conduction currents and displacement currents in the complex permittivity $\tilde{\varepsilon}$. This allows us to give a unified treatment of EM-field decomposition in both conductive ($\sigma \neq 0$) and nonconductive ($\sigma = 0$) media. The characteristic frequency at which the conduction current equals the displacement current is $\omega_0 = \sigma/\varepsilon$. For conductive media, the ratio ω_0/ω plays an important role in determining how lossy the medium is in terms of the field's at-

tenuation with propagation distance. The field-decomposition theory presented below is valid for any type of lossy medium. It applies to multicomponent GPR data, as well as to SBL measurements.

For SBL data, which is the case of main interest in this paper, conductivity (or its reciprocal, resistivity) of seawater depends on salinity and temperature, and it typically is in the range $\sigma \sim 1$–5 S/m. Salinity varies from sea to sea, but in most major oceans it is 3.5% by weight. At 0°C, the resistivity is approximately 0.34 Ωm, and the conductivity is 2.94 S/m. With an electric permittivity of 80 ε_0, where $\varepsilon_0 = 8.854 \times 10^{-12}$ F/m is the permittivity of free space, the ratio is $\omega_0/\omega \approx 6.61 \times 10^8/f$, where f is the frequency of the field. Probing the earth with low-frequency signals, typically of a few tenths to a few tens of hertz, shows that seawater is a good conductor. To a good approximation,

$$\tilde{\varepsilon} = \frac{i\sigma}{\omega} \tag{14}$$

is independent of the electric permittivity. For field decomposition on the seabed, we set the magnetic permeability μ to that of free space ($\mu = \mu_0 = 4\pi \times 10^{-7}$ H/m), which is representative of the water layer and a nonmagnetic seabed. The complex velocity then is

$$\tilde{c} = \sqrt{\frac{\omega}{i\mu_0\sigma}}. \tag{15}$$

The frequency dependence of the velocity leads to strong dispersion and attenuation. The phase velocity is given by $c_{ph} = \omega/\text{Re}(k)$, where the wavenumber k representative for the EMSBL experiment is given in equation A-17. Using that $\text{Re}(k) = \sqrt{\omega\mu\sigma/2}$ gives

$$c_{ph} = \sqrt{\frac{2\omega}{\mu_0\sigma}}. \tag{16}$$

For the above conductivity value of seawater at a frequency of 0.25 Hz, the phase velocity in seawater is $c_{ph} \approx 922$ m/s. The skin depth δ, where the EM field will be reduced in amplitude by a factor of $1/e$, is

$$\delta = \sqrt{\frac{2}{\omega\mu_0\sigma}}. \tag{17}$$

At the frequency of 0.25 Hz, the skin depth in the seawater example is $\delta \approx 586$ m.

DECOMPOSITION INTO UPGOING AND DOWNGOING FIELDS

For an electric dipole source in a 3D homogeneous medium, it intuitively follows that four independent field solutions must exist: two above the source, propagating upward as electric and magnetic components, and two below the source, propagating downward as electric and magnetic components. The nature of the source determines their amplitudes. Generally, the electric and magnetic fields consist of components traveling both upward U and downward D, and we therefore can write

$$\boldsymbol{\mathcal{E}} = \boldsymbol{\mathcal{E}}^{(U)} + \boldsymbol{\mathcal{E}}^{(D)} \tag{18}$$

and

$$\mathcal{H} = \mathcal{H}^{(U)} + \mathcal{H}^{(D)}. \tag{19}$$

To derive the relationship between the electric and magnetic fields and their upgoing and downgoing constituents, it is useful to find the eigensolutions of the system matrix $\mathbf{A}$, i.e., the solutions of the equation

$$\mathbf{A}\mathbf{l}_N = \lambda_N \mathbf{l}_N, \quad N = 1,2,3,4, \tag{20}$$

where λ_N is the eigenvalue and $\mathbf{l}_N$ is the eigenvector that corresponds to λ_N. The four eigenvalues

$$\lambda_1 = \lambda_2 = -\lambda_3 = -\lambda_4 = -q = -\sqrt{\tilde{c}^{-2} - p^2} \tag{21}$$

can be grouped into the 4×4 diagonal matrix

$$\mathbf{\Lambda} = \mathrm{diag}[\lambda_1, \lambda_2, \lambda_3, \lambda_4] = -q\,\mathrm{diag}[1, 1, \ -1, \ -1]. \tag{22}$$

Likewise, we form a 4×4 matrix with the eigenvectors as columns:

$$\mathbf{L} = [\mathbf{l}_1, \mathbf{l}_2, \mathbf{l}_3, \mathbf{l}_4]. \tag{23}$$

The eigensolution given in equation 20 then can be written

$$\mathbf{A}\mathbf{L} = \mathbf{L}\mathbf{\Lambda}. \tag{24}$$

In a homogeneous region of space, the system matrix $\mathbf{A}$ is constant, and so the eigenvector matrix $\mathbf{L}$ is independent of x_3. The first-order differential equation 5 for the electric-magnetic-field vector $\mathbf{b}$ then can be transformed into the first-order differential equation,

$$\partial_3(\mathbf{L}^{-1}\mathbf{b}) = i\omega\mathbf{\Lambda}(\mathbf{L}^{-1}\mathbf{b}). \tag{25}$$

By introducing the 4×1 column vector,

$$\mathbf{w} = \mathbf{L}^{-1}\mathbf{b}, \tag{26}$$

equation 25 yields one-way, decoupled differential equations for each of the elements of $\mathbf{w}$, which is seen to represent differential equations for two upward-propagating fields and two downward-propagating fields. Thus, the entries of $\mathbf{w}$ are upgoing and downgoing fields. The normalization of the eigenvectors remains a degree of freedom. By a special eigenvector normalization, one can obtain

$$\mathbf{w} = \mathbf{L}^{-1}\mathbf{b} = [\boldsymbol{\mathcal{E}}^{(U)T}, \boldsymbol{\mathcal{E}}^{(D)T}]^T. \tag{27}$$

The effect of $\mathbf{L}^{-1}$ is to decompose the EM-field vector into upgoing and downgoing components. Therefore, $\mathbf{L}^{-1}$ is called the decomposition matrix. Note that the decomposition simply is a linear transformation of the physical variables and therefore is a stable process. The inverse relation of equation 26 is

$$\mathbf{b} = \mathbf{L}\mathbf{w}. \tag{28}$$

The effect of $\mathbf{L}$ is to compose the electric-magnetic field vector from the upgoing and downgoing components; $\mathbf{L}$ is called the composition matrix.

In wave-equation theory, λ_N represents the phase slowness and $\mathbf{l}_N$ represents the polarization vector (see, e.g., Ikelle and Amundsen, 2005). The polarization vector $\mathbf{l}_N$ consists of two two-component vectors, one that corresponds to the horizontal components of the electric field $(E_1, E_2)^T$ and another that corresponds to the horizontal components of the magnetic field $(-H_2, H_1)^T$. The subscript N indicates the wavetype: $N = 1$ corresponds to an upgoing wave in the x_1-direction, $N = 2$ corresponds to an upgoing wave in the x_2-direction,

$N = 3$ corresponds to a downgoing wave in the x_1-direction, and $N = 4$ corresponds to a downgoing wave in the x_2-direction.

UPGOING AND DOWNGOING CONSTITUENTS OF E_1 AND E_2

Our task is to analytically describe the matrix $\mathbf{L}$ and its inverse. To this end, we need to determine the eigenvectors $\mathbf{l}_N$ from equation 20. As stated above, we are free to scale the eigenvectors so that the upgoing and downgoing wave variables represent the electric (or magnetic) field. Ursin (1983) scaled them with respect to the vertical energy flux. This yields symmetry properties that may be used in the analysis of reflection and transmission responses of a layered medium. Here, we scale with respect to the amplitude of the electric field.

Solving equation 20, and scaling the eigenvectors so that $\mathbf{w}$ represents the electric field, we find the composition matrix,

$$\mathbf{L} = \begin{bmatrix} \mathbf{I} & \mathbf{I} \\ \boldsymbol{\mathcal{L}} & -\boldsymbol{\mathcal{L}} \end{bmatrix}, \tag{29}$$

with its inverse, the decomposition matrix,

$$\mathbf{L}^{-1} = \frac{1}{2}\begin{bmatrix} \mathbf{I} & \boldsymbol{\mathcal{L}}^{-1} \\ \mathbf{I} & -\boldsymbol{\mathcal{L}}^{-1} \end{bmatrix}, \tag{30}$$

where $\mathbf{I}$ is the 2×2 identity matrix and where

$$\boldsymbol{\mathcal{L}} = \frac{1}{\mu q}\begin{pmatrix} q_2^2 & p_1 p_2 \\ p_1 p_2 & q_1^2 \end{pmatrix}, \quad \boldsymbol{\mathcal{L}}^{-1} = \frac{1}{\tilde{\varepsilon}q}\begin{pmatrix} q_1^2 & -p_1 p_2 \\ -p_1 p_2 & q_2^2 \end{pmatrix}. \tag{31}$$

From equation 27, we compute the upgoing and downgoing electric fields,

$$\boldsymbol{\mathcal{E}}^{(U)} = \frac{1}{2}(\boldsymbol{\mathcal{E}} + \boldsymbol{\mathcal{L}}^{-1}\boldsymbol{\mathcal{H}}) \tag{32}$$

and

$$\boldsymbol{\mathcal{E}}^{(D)} = \frac{1}{2}(\boldsymbol{\mathcal{E}} - \boldsymbol{\mathcal{L}}^{-1}\boldsymbol{\mathcal{H}}) = \boldsymbol{\mathcal{E}} - \boldsymbol{\mathcal{E}}^{(U)}, \tag{33}$$

respectively. Observe that equation 18 is fulfilled. In component form, the upgoing constituents of E_1 and E_2 are

$$E_1^{(U)} = \frac{1}{2}\left[E_1 - \frac{1}{\tilde{\varepsilon}q}(p_1 p_2 H_1 + q_1^2 H_2)\right] \tag{34}$$

and

$$E_2^{(U)} = \frac{1}{2}\left[E_2 + \frac{1}{\tilde{\varepsilon}q}(p_1 p_2 H_2 + q_2^2 H_1)\right], \tag{35}$$

respectively. The scalars in front of the electric- and magnetic-field components are called decomposition scalars. The upgoing constituents of E_1 and E_2 will not contain any downgoing reflections and refractions caused by the sea surface, nor will they receive the direct field from the source because the receivers are below the source. After decomposing the measured EM field into upgoing and downgoing constituents, the sea-surface reflections and refractions and the direct-source field will belong only to the downgoing part of the

fields, $E_i^{(D)} = E_i - E_i^{(U)}$, $i = 1, 2$. Most MT noise that is present during the survey also will be in the downgoing component. Only the much weaker reflected MT field will remain in the upgoing field. The upgoing and downgoing fields may be inverse Fourier transformed to the space and time domains by using equation 4.

Equations 34 and 35 are the most general formulas for EM-field decomposition of the electric-field components into upgoing fields. The schemes require that the receiver stations be distributed over an area so that the EM field can be Fourier transformed to the frequency-wavenumber domain. These decomposition schemes, equations 34 and 35, are valid for a 3D inhomogeneous earth.

Special case: $p_2 = 0$

When the EMSBL experiment is run along a single profile, data are available only along a line. The electric-field components E_1 and E_2 then can be properly decomposed into upgoing and downgoing components under the 2.5D-earth assumption of no variations in the parameters of the earth in the cross-profile direction. Without loss of generality, we orient the coordinate system so that the EM field propagates in the x_1, x_3-plane, such that $p_2 = 0$. Then, $q_2 = \tilde{c}^{-1}$, and $q = q_1$ inserted into equation 34 gives

$$E_1^{(U)} = \frac{1}{2}\left(E_1 - \frac{q_1}{\tilde{\varepsilon}}H_2\right). \tag{36}$$

Equation 36 shows that computing the upgoing constituent of the E_1 field component requires combining the E_1 recording with a scaled H_2 magnetic-field component. Similarly, the upgoing component of the E_2 field is

$$E_2^{(U)} = \frac{1}{2}\left(E_2 + \frac{\mu}{q_1}H_1\right). \tag{37}$$

Equations 36 and 37 are valid only under the 2.5D-earth assumption; however, for single-profile data over a 3D earth, equations 36 and 37 still can be used as an approximate method to attenuate downgoing energy on the electric E_1 and E_2 components.

Note, however, that transforming line-profile data to the slowness or wavenumber domain requires a Hankel transform. Such a plane-wave decomposition is valid for a horizontally layered earth response.

For the 2D diffusion equation, the equivalent of equation 37 was derived by Zhdanov et al. (1996, equation A-3).

Special case: $p_1 = p_2 = 0$

The special case of vertically traveling EM plane waves with $p_1 = p_2 = 0$, such that $q_1 = q_2 = q = \tilde{c}^{-1}$, by substitution into equations 34 and 35 yields

$$E_1^{(U)} = \frac{1}{2}\left(E_1 - \frac{1}{\tilde{c}\tilde{\varepsilon}}H_2\right) \tag{38}$$

and

$$E_2^{(U)} = \frac{1}{2}\left(E_2 + \frac{1}{\tilde{c}\tilde{\varepsilon}}H_1\right). \tag{39}$$

In this case, the decomposition scalar to be applied to the magnetic components simply is proportional to the local EM impedance

$(\tilde{c}\tilde{\varepsilon})^{-1}$. For EMSBL data, one uses $(\tilde{c}\tilde{\varepsilon})^{-1} = \sqrt{\omega\mu_0/\sigma}\exp(-i\pi/4)$. Even though equations 38 and 39 are valid only for vertically traveling plane waves, they also can be useful approximations for wave-field decomposition for nonvertically traveling plane waves. Note that the components $E_1^{(U)}$ and $E_2^{(U)}$ will not contain any vertically downward-traveling noise. Therefore, equations 38 and 39 represent attractive and very simple processing schemes for noise reduction, particularly for the attenuation of the source-induced airwave and MT noise. Because the decomposition scalar applied to the magnetic components does not depend on slowness, equation 38 can be implemented directly in the space domain.

Equations 38 and 39 show that the decomposition simply is a linear combination of the electric and scaled magnetic fields and thus is a fully stable process.

For the 1D diffusion equation, the equivalent of equation 38 was given by Levy et al. (1988, equation 5), and the equivalent of equation 39 was given by Zhdanov et al. (1996, equation A-6).

UPGOING AND DOWNGOING CONSTITUENTS OF H_1 AND H_2

To find the upgoing and downgoing constituents of H_1 and H_2, one can scale the polarization vectors in equation 20 so that **w** represents the magnetic field according to equation 19. There also is a simpler procedure. For a purely upgoing field, equation 28 gives the relationship between the magnetic and electric fields:

$$\mathcal{H}^{(U)} = \mathcal{L}\mathcal{E}^{(U)}. \tag{40}$$

Likewise, for a purely downgoing field, the relation is

$$\mathcal{H}^{(D)} = -\mathcal{L}\mathcal{E}^{(D)}. \tag{41}$$

Combining equations 40 and 41 with equations 32 and 33 yields

$$\mathcal{H}^{(U)} = \frac{1}{2}(\mathcal{H} + \mathcal{L}\mathcal{E}) \tag{42}$$

and

$$\mathcal{H}^{(D)} = \frac{1}{2}(\mathcal{H} - \mathcal{L}\mathcal{E}) = \mathcal{H} - \mathcal{H}^{(U)}. \tag{43}$$

In component form, we find that the upgoing constituents of H_1 and H_2 become

$$H_1^{(U)} = \frac{1}{2}\left[H_1 + \frac{1}{\mu q}(p_1 p_2 E_1 + q_1^2 E_2)\right] \tag{44}$$

and

$$H_2^{(U)} = \frac{1}{2}\left[H_2 - \frac{1}{\mu q}(p_1 p_2 E_2 + q_2^2 E_1)\right], \tag{45}$$

respectively. The components $H_1^{(U)}$ and $H_2^{(U)}$ will not contain downgoing signals related to the source, to the sea surface, or to incoming MT noise. The upgoing and downgoing fields may be inverse Fourier transformed to the space and time domains by using equation 4.

As for the case with the electric-field components, equations 44 and 45 are the general formulas for the upgoing magnetic-field components. The schemes require that the receiver stations be distributed over an area on the seabed so that the EM field can be Fourier

transformed to the frequency-wavenumber domain. These decomposition schemes, equations 44 and 45, are valid for a 3D inhomogeneous earth.

Special case: $p_2 = 0$

When the EMSBL experiment is run along a single profile, data are available only along a line. Under the 2.5D assumption stated above for the electric field for the special case $p_2 = 0$, the upgoing constituents of the magnetic field become

$$H_1^{(U)} = \frac{1}{2}\left(H_1 + \frac{q_1}{\mu}E_2\right) = \frac{q_1}{\mu}E_2^{(U)} \qquad (46)$$

and

$$H_2^{(U)} = \frac{1}{2}\left(H_2 - \frac{\tilde{\varepsilon}}{q_1}E_1\right) = -\frac{\tilde{\varepsilon}}{q_1}E_1^{(U)}. \qquad (47)$$

Special case: $p_1 = p_2 = 0$

In the special case of vertically traveling EM plane waves with $p_1 = p_2 = 0$, equations 44 and 45 give

$$H_1^{(U)} = \frac{1}{2}(H_1 + \widetilde{c\varepsilon}E_2) = \widetilde{c\varepsilon}E_2^{(U)} \qquad (48)$$

and

$$H_2^{(U)} = \frac{1}{2}(H_2 - \widetilde{c\varepsilon}E_1) = -\widetilde{c\varepsilon}E_1^{(U)}. \qquad (49)$$

The decomposition scalar is proportional to the reciprocal of the local electromagnetic impedance. The comments given for the decomposition of the electric field for $p_1 = p_2 = 0$ also are valid for these decompositions, equations 48 and 49.

For the 1D diffusion equation, the equivalent of equation 49 has been given by Zhdanov et al. (1996, equation A-9).

UPGOING AND DOWNGOING CONSTITUENTS OF E_3 AND H_3

The upgoing and downgoing constituents of E_3 and H_3 are straightforwardly determined by using Maxwell's equations:

$$E_3^{(U)} = \tilde{\varepsilon}^{-1}(p_2 H_1^{(U)} - p_1 H_2^{(U)}), \quad (50)$$

$$E_3^{(D)} = E_3 - E_3^{(U)}, \qquad (51)$$

$$H_3^{(U)} = \mu^{-1}(p_1 E_2^{(U)} - p_2 E_1^{(U)}), \quad (52)$$

and

$$H_3^{(D)} = H_3 - H_3^{(U)}. \qquad (53)$$

Introducing equations 34, 35, 44, and 45 for the upgoing horizontal components, one finds (see Røsten and Amundsen, 2004)

$$E_3^{(U)} = \frac{1}{2}\left[E_3 + \frac{1}{q}(p_1 E_1 + p_2 E_2)\right] \qquad (54)$$

and

$$H_3^{(U)} = \frac{1}{2}\left[H_3 + \frac{1}{q}(p_1 H_1 + p_2 H_2)\right]. \qquad (55)$$

DATA EXAMPLES

The multidimensional field-decomposition theory presented in this paper has been developed for both conductive and nonconductive media. However, here we consider specifically the field decomposition of SBL data. First, we illustrate and verify the performance of the decomposition technique by using 3D synthetic data: For one source location, we use a frequency-wavenumber-domain algorithm for 3D field propagation over a horizontally layered medium (Løseth, 2000) to model data into receivers distributed over an area of the seafloor. Second, we demonstrate the current practice of 1D field ($p_1 = p_2 = 0$) decomposition just below the seabed to SBL electric and magnetic data recorded in shallow water (320 m) over the giant Troll gas field offshore Norway. The key decomposition formula then is equation 38, with $(\widetilde{c\varepsilon})^{-1} = \sqrt{\omega\mu_0/(i\sigma)}$. The decomposition is applied to common receiver gathers, where data are acquired as time series and then are processed by a windowed Fourier-series analysis. To calculate the decomposition scalar, the local electric conductivity σ of the seabed must be known or estimated.

The reservoir interval of the Troll field is Jurassic sandstones with a gas column up to 160 m. Reservoir overburden in the SBL survey area is 1100–1200 m. Gas-filled reservoir intervals have resistivities of approximately 70 Ωm, whereas water-bearing sands and overburden sediments generally show resistivities in the 0.5–2 Ωm range (Amundsen et al., 2004). Detailed descriptions of the geology of the Troll field are published by Osborne and Evans (1987), as well as by others. Figure 3 shows a representative geological cross-section of the area where the SBL survey was run. Observe the simple overburden of gently dipping layers.

Before we move on to the synthetic-data example, we reiterate that even though the model used to generate synthetic data is horizontally layered, the field-decomposition theory is valid for SBL recordings from any complex subsurface. The major assumption is that the data were measured on a plane where the electric conductivi-
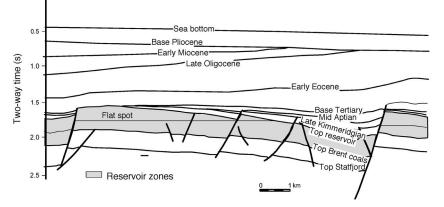

Figure 3. Troll field geological cross section that is representative of the area where the SBL survey was conducted. Observe that the overburden is very simple.

ty is constant with respect to space. Above and below the plane of measurement, the medium can be arbitrarily inhomogeneous and anisotropic.

Synthetic data

For the simulation of synthetic data, we constructed a layered model on the basis of SBL inversion (see Mittet et al., 2004) that is representative of the area where the real SBL survey was run along a 2D line. The model's water depth is 320 m. Below the seabed, the water-bearing sands and overburden of approximately 1150 m are given resistivities in the 0.5–2 Ωm range. For the reservoir zone, we use two different models. In the first model, no gas is present. The water-filled reservoir zone has resistivities similar to those of the overburden. In the second model, the reservoir zone is assumed to be filled with gas, with resistivities in the reservoir of approximately 70 Ωm.

The dipole source has a sine-wave signal of 0.25 Hz. In the following, even though data have been modeled into a grid of seabed sensors, for display purposes we show only data for one station re-
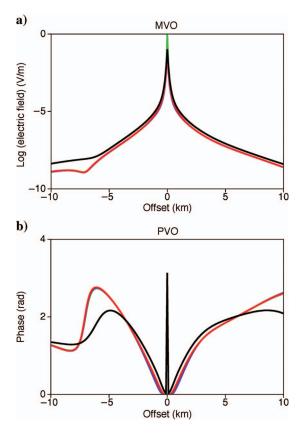

Figure 4. Field separation just above the seabed of the synthetic electric field, without (negative offsets) and with (positive offsets) the presence of a hydrocarbon-filled reservoir. (a) MVO spectra and (b) PVO spectra are shown for the full electric field (black line), its modeled upgoing component (green line, beneath the black line), its numerically decomposed upgoing component that was computed using equation 34 (black line), and the special case $p_1 = p_2 = 0$ upgoing component that was computed using equation 38 (red line). For all offsets, the green line is directly beneath the black line and therefore cannot be seen. In this model, for offsets larger than ±3 km, the decomposition results according to equations 34 and 38 are almost equal, which is indicated by the coinciding red and black curves. (The red line is on top of black line.)

ceiver, as magnitude variation with offset (MVO) and phase variation with offset (PVO) spectra sections at the transmitted frequency for one sail line passing above the receiver. The offset range is from −10 km to +10 km. In the presentation of MVO and PVO curves, to better distinguish between the effects of gas absent and gas present in the data, we let the negative offsets correspond to the model with the high-resistivity layer absent (no gas), and we let the positive offsets correspond to the model with the high-resistivity layer present (gas).

Løseth's (2000) 3D wavenumber-domain-modeling algorithm allows the computation in the space domain of the EM-field components (E_1, E_2, H_1, H_2) on the seabed. The algorithm first computes in the wavenumber domain the reflection responses for TM and TE modes. Next, the modes are Bessel transformed to the space domain by adaptive numerical evaluation of integrals with upper infinite integration limits. Then, the space domain results are synthesized to the proper physical fields. Figure 4 displays in black lines the MVO and PVO spectra for the modeled electric-field component E_1. (The other field components are not shown.) The task now is to decompose E_1 into upgoing and downgoing constituents, according to the decomposition algorithm, equation 34. After the modeled data are Fourier transformed to the wavenumber domain using equation 3, the transformed data are weighted by the appropriate decomposition scalars before being summed according to equation 34. An inverse-Fourier transform (equation 4) of the decomposed wavenumber-domain responses then yields the decomposed space-domain data. The blue lines in Figure 4 present the MVO and PVO spectra for the numerically decomposed upgoing component $E_1^{(U)}$. The computation is numerically stable because the decomposition amounts to computing specific linear combinations of the EM fields.

The modeling algorithm described in Løseth (2000) allows the simulation, just above the seabed, of the upgoing and downgoing components of the EM field. The modeling algorithm therefore is used to verify that all constituents output from the decomposition algorithm are correct. Figure 4 displays the modeled upgoing $E_1^{(U)}$ component (green line). Except around zero offset in the MVO plot, the green line cannot be seen because it is beneath the blue line, thus verifying the correctness and stability of the decomposition method. Although both algorithms involve computations in the wavenumber domain, the numerical integral transforms involved in the decomposition algorithm and in the modeling algorithm differ. Whereas the modeling algorithm uses Bessel transforms to synthesize data in the space domain, the decomposition algorithm uses Fourier transforms to decompose the data into plane waves. Therefore, the Fourier transform of modeled spatial data to the wavenumber domain will not give exactly those wavenumber data that were numerically modeled.

The 1D special case $p_1 = p_2 = 0$ upgoing $E_1^{(U)}$ component can easily be computed in the space domain from E_1 and H_2 using equation 38. Evaluated just above the seabed, for comparison with the above decomposed field result that is shown by the blue lines, the 1D decomposed MVO and PVO spectra are displayed as red lines in Figure 4. In this model, studying the PVO spectrum, we observe that for offsets larger than approximately ±3 km, the decomposition results from equations 34 and 38 are almost equal.

Recall that the SBL method is devised to detect and characterize hydrocarbon-bearing layers by using EM energy that is recorded at large offsets. When the EM signal encounters a high-resistivity layer embedded in a much-less-resistive background, EM energy is partly guided along the layer that has lower attenuation than the signal trav-

eling outside the high-resistivity layer. Because of the high velocity contrast between the background and the high-resistivity layer, the observed seabed EM signal at large offsets can be considered to be just above the seabed and to consist of rays that are traveling close to the vertical axis, typically at less than 10°–15°. The airwave, on the other hand, has an angle of incidence almost at 0°. Therefore, one should expect that the 1D decomposition schemes (equations 38, 39, 48, and 49) at large offsets that are evaluated above the seabed are good approximations to full field decomposition of the two most significant modes in shallow-water hydrocarbon-layer detection. The synthetic-data example illustrates this aspect by comparing the results from exact and approximate 1D field decomposition at large offsets.

Note that, for larger offsets, the amplitudes are greater above the high-resistivity gas reservoir (positive offsets) than they are outside the gas reservoir (negative offsets). Because the models are otherwise equal, this response is attributable solely to the gas-filled reservoir, and thus is a direct hydrocarbon identifier. (See the later discussion of Figure 6 for a more visual description of this response of hydrocarbons.)

The PVO curvature change at approximately −6 km offset in Figure 4b can be explained as a rollover in the signal from events that have dominantly low phase velocities at short offsets to the airwave event with high phase velocity at large offsets. In general, the recorded field at any offset in marine-EM surveying is a sum of many events, including reflections or refractions from the subsurface. Occasionally there are contributions from high-resistivity layers. Also, there is a significant airwave contribution for shallow water. The phase of the recorded data depends on the complex amplitude of the sum of these events. It therefore is a full-scale inverse problem to relate the measured phase to the medium properties. If, however, one event is much stronger than the other events, then the phase also is dominated by this strong event. Furthermore, the phase is approximately proportional to the circular frequency divided by the phase velocity times the offset. Thus, the phase gradient with respect to offset is proportional to the circular frequency divided by the phase velocity.

In Figure 4b, at short offsets, the modeled field is dominated by the direct wave and the shallow refractions. These events have a low phase velocity, which leads to a relatively steep PVO gradient with offset. The airwave, on the other hand, has a large phase velocity, which leads to a small gradient in phase with respect to offset. At offsets greater than approximately −8 km in Figure 4b, the airwave dominates; hence, there is a small phase gradient. In the offset interval from approximately −5 km to −8 km, the relative importance of the airwave increases; thus, the airwave starts to dominate the shallower refraction events of the signal. In this particular offset interval, the phase curve shows rollover from dominant events with low phase velocities to the airwave event with large phase velocity. The rollover effect also is present in the decomposed upgoing components. Recall that in this particular data example, the decomposition is performed just above the seabed, where the airwave has an upward-reflected mode caused by the contrast in conductivity across the seabed.

On real data, because today's data acquisition geometries are optimized toward cost-effective exploration rather than toward data-processing theory, the current practice of field decomposition is based on the special case $p_1 = p_2 \approx 0$ decomposition evaluated just below the seabed using equation 38. Figure 2 shows why field decomposition in shallow water is preferred below rather than above

the seabed: Below the seabed, the source-induced airwave component, always traveling with $p_1 = p_2 = 0$, is downgoing. Figure 5 displays (dashed red line) the MVO and PVO spectra of $E_1^{(U)}$ that were computed just below the seabed using equation 38. For reference, the corresponding component that was computed just above the seabed is shown by the red line (identical to the one in Figure 4). The full modeled field once more is plotted in black line. In the MVO section, for positive offsets and for negative offsets up to −6 km, the dashed red line is hidden beneath the black line. The effect of the elimination of the source-induced airwave component can be seen in the MVO spectrum for offsets greater than −6 km, but it is most striking in the PVO display. A PVO comparison of black and dashed red lines at large negative offsets, where the effect of the high-resistivity reservoir is absent, shows that the electric field is dominated by the extremely high-speed source-induced airwave component. After the airwave component is eliminated by the up/down decomposition, the phase spectrum (dashed red line) shows an almost linear phase, which is characteristic of low-speed events from the subsurface. At large positive offsets, where the high-resistivity reservoir is present, the electric field (black line) will be dominated by two high-speed components: the source-induced airwave and the hydrocarbon-lay-
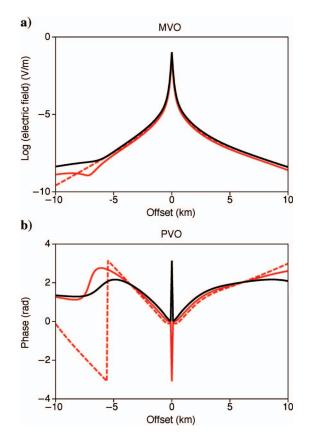

Figure 5. Field separation just below the seabed of the synthetic electric field, without (negative offsets) and with (positive offsets) the presence of a hydrocarbon-filled reservoir. (a) MVO spectra and (b) PVO spectra are shown for the full electric field (black line) and for the special case $p_1 = p_2 = 0$ upgoing component that was computed using equation 38 (dashed red line). For comparison, the red line, identical to the one in Figure 4, shows the special case $p_1 = p_2 = 0$ upgoing component just above the seabed. In the MVO plot, for positive offsets and for negative offsets of up to −6 km, the dashed red line accidentally is hidden beneath the black line.

er-guided event constantly leaking energy to the seabed receivers. The elimination of the airwave component, again achieved by the up/down decomposition, equation 38, shows through the linear characteristic of the phase spectrum (in dashed red line) for large offsets that the upgoing field below the seabed is dominated by one high-speed component: the refraction event from the reservoir. The phase-spectra plots indicate that the airwave component starts to influence the electric field at offsets greater than ±3 km.

SBL data can be analyzed further by comparing the measured response from the hydrocarbon (gas) reservoir to a reference response from the nonreservoir area. One common analysis technique is to normalize the offset amplitude measured in the common-receiver gather above the potential reservoir with respect to the same offset amplitude recorded in a common-receiver gather outside the reservoir. For the synthetic data displayed in Figure 5, the normalized MVO response shown in Figure 6 begins to deviate from unity at offsets larger than 3 km. The black line gives the normalized MVO response for the full electric field, and the dashed-red and solid-red lines show the corresponding normalized responses for the $p_1 = p_2 = 0$ upgoing components below and above the seabed, respectively. Any significant deviation from unity of the MVO response allows the identification of the high-resistivity hydrocarbon (gas) reservoir. The deviation is markedly greater with field decomposition than it is without field decomposition, illustrating the potential of the simple decomposition scheme, equation 38, for improving SBL-data quality.

Real data

In this subsection, we demonstrate the current practice of 1D field decomposition just below the seabed to a common-receiver SBL gather recorded above the Troll gas province offshore Norway in an area with relatively flat layers, as shown in Figure 3. The water depth is approximately 320 m. Because the two models used in the above subsection to some extent are representative for this area, the synthetic-data results and their interpretation will support the interpretation of the real-data results that soon will be presented.

The SBL survey is performed by dropping electric and magnetic

sensors on the seabed along a predetermined sail line, and then towing a horizontal electric dipole along the line. The dipole source transmits a continuous square pulse at a fundamental frequency of 0.25 Hz. In the survey, the EM fields are recorded as time series while the source vessel is passing over the stationary recording units. Because of the limited dynamic range in the recording system for this particular experiment, the data for small source-receiver distance are clipped.

Below, we consider the measurements of E_1 and H_2 at one station receiver that is deployed on the seafloor above the edge of the gas province that has high resistivity inside the gas-filled layer, but low resistivity outside. For positive offsets, the dipole transmitter in the out-towing direction traverses the gas province so that a strong guided and refracted response from the reservoir can be expected at large offsets. For negative offsets, the dipole transmitter traverses in the in-towing direction outside the gas province, so that no strong response from the subsurface is expected. In both cases, the effect of the airwave component will be observable at moderate to large offsets.

Similarly to the synthetic-data displays, Figure 7 shows in black lines the MVO and PVO spectra for the SBL electric-field component E_1. Except for small offsets, where the SBL data have suffered

Figure 7. Field separation just below the seabed of the SBL electric field, without (negative offsets) and with (positive offsets) the presence of a hydrocarbon-filled (gas) reservoir. (a) MVO spectra and (b) PVO spectra are shown for the full electric field (black line) and for the special case $p_1 = p_2 = 0$ upgoing component that was computed using equation 38 (dashed red line). Except for small offsets, where the SBL data suffered amplitude clipping, the offset behavior of the magnitude and phase spectra agree qualitatively with the corresponding spectra in Figure 5.
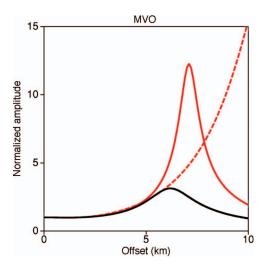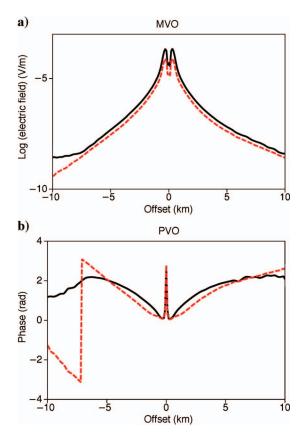

Figure 6. Normalized MVO response for the synthetic data shown in Figure 5: the full electric field (black line), and the special case $p_1 = p_2 = 0$ upgoing component that was evaluated below (dashed red line) and above (red line) the seabed.

amplitude clipping, the offset behavior of the MVO and PVO spectra reasonably agree qualitatively with the corresponding synthetic spectra in Figure 5. Observe that for larger offsets, the amplitudes are greater for positive offsets above the high-resistivity gas reservoir than for negative offsets outside the gas reservoir. This difference, which is a direct hydrocarbon identifier, is more pronounced in Figure 8, which we will discuss shortly.

We now apply the 1D decomposition formula, equation 38, just below the seabed to the SBL data. The result is shown in dashed red lines in Figure 7. Compared to the recorded field, the computed upgoing component at large negative offsets has a decaying behavior, indicating that the airwave component has been successfully removed. When the airwave component is present and dominates the data, which is the case in shallow water for large offsets outside any high-resistivity layers, the MVO curve is expected to flatten because of the geometrical behavior of the airwave component. In this geological area, for the large positive offsets, on the other hand, the guided wave component from the gas reservoir contributes significantly to the full field, and thus it dominates the effect of the airwave component. Figure 5 shows that the same behavior of MVO curves is observed in the synthetics.

As did the synthetic-PVO spectra shown in Figure 5, the real-data PVO spectra in Figure 7 further strengthen this interpretation. At large negative offsets, where the gas reservoir is absent, the electric field is dominated by the high-speed source-induced airwave component. After elimination of the airwave, the phase spectrum shows an almost linear phase, which is characteristic of low-speed events related to the subsurface. At large positive offsets, where the gas reservoir is present, the electric field is expected to be dominated by two high-speed components: the source-induced airwave and the hydrocarbon-layer guided event. The elimination of the airwave component is evident in the phase spectrum's linear characteristics. For large positive offsets, the upgoing electric-field component below the seabed is dominated by one high-speed component: the event from the gas reservoir.

Finally, Figure 8 shows the normalized MVO curves related to the measured E_1 component (black line) and its upgoing $E_1^{(U)}$ component that was evaluated just below the seabed (dashed red line). For large offsets, the deviation from unity is significant for both curves. Even without applying any field decomposition, we observe that at offsets of 7–8 km, the magnitude spectrum above the gas reservoir is as much as three times higher than it is outside the gas reservoir. However, the gas-presence effect is especially prominent in the normalized MVO curve of the upgoing component. Whereas the normalized MVO curve of the E_1 field shows decreasing amplitudes with offsets greater than 7 km, the normalized amplitude that corresponds to the $E_1^{(U)}$ component still increases strongly with offset. This effect is attributed to the attenuation of the airwave component. This result shows the importance of using field decomposition to attenuate downgoing modes before undertaking further data processing and interpretation of SBL data.

FUTURE WORK

This paper presents a theory for decomposition of EM fields into their upgoing and downgoing components. One synthetic- and one real-data example are presented to illustrate the potential of the decomposition algorithm. However, because SBL data acquisition and related data processing still are in their infancy, more investigation is needed to evaluate the full impact of field decomposition for data in-
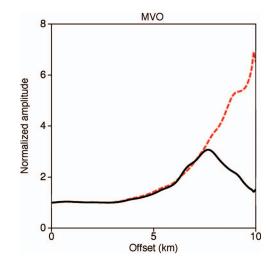

Figure 8. Normalized MVO response for the SBL data shown in Figure 7: the full electric field (black line) and the special case $p_1 = p_2 = 0$ upgoing component that was evaluated below the seabed (dashed red line). Note the similarity of this MVO response to the one in Figure 6 (black and dashed red lines).

terpretation. Ongoing and planned future work is related to (1) implementation and evaluation of the special case $p_2 = 0$ decomposition algorithms, equations 37 and 46; (2) evaluation of decomposition algorithms applied above and below the seabed for various seabed properties and near-surface resistivity profiles; (3) further development of calibration schemes for EMSBL measurements; and (4) elimination of the full water-layer response from EMSBL data.

CONCLUSIONS

Using Maxwell's equations, we have given a unified treatment of EM-field decomposition into upgoing and downgoing components for conductive and nonconductive media where the EM data are measured on a plane where the electric permittivity, magnetic permeability, and electrical conductivity are constant with respect to space and time. Above and below the plane of measurement, the medium can be arbitrarily inhomogeneous and anisotropic.

The field-decomposition analysis yields expressions in which slowness-dependent (or wavenumber-dependent) decomposition scalars are multiplied with the EM data that have been Fourier transformed to the slowness (or wavenumber) domain. After field decomposition, the data are inverse-Fourier transformed to the space domain for further processing, analysis, and interpretation. For vertically traveling plane waves, the decomposition scalar is independent of slowness. For the electric components, the scalar is proportional to the reciprocal of the local impedance, whereas for the magnetic components, the scalar is proportional to the local impedance. Field decomposition then can be done directly in the space domain. In this case, the upgoing and downgoing separation is performed for each station receiver in the EM experiment.

The numerical examples clearly demonstrated the potential impact of applying field decomposition methods to marine low-frequency EMSBL data acquired in shallow water. The real-data example reveals that the gas reservoir's presence is systematically stronger in the normalized MVO spectrum for large offsets with field decomposition than for those without it. The decomposition methods

that we describe in this paper promise to open a new frontier in shallow-water SBL hydrocarbon mapping.

APPENDIX A

EMSBL ALGORITHMS:
WAVE OR DIFFUSION PERSPECTIVE?

This appendix shows that the EMSBL field can be analyzed using its wave character, and that the field's diffusive character is a special case of its wave character. The implication of this well-known observation is that the mathematical formulation of EMSBL modeling and processing methods can be given in terms of the wave-theory apparatus. In this paper, we use the wave-theoretical approach to develop a mathematical scheme to decompose the EMSBL field into upgoing and downgoing components. To implement it on a computer, simply reduce the complex permittivity and the complex velocity to their appropriate very-low-frequency limits as given in equations 14 and 15.

Consider the EM field in a region characterized by the material parameters μ and ε, and by the finite electrical conductivity σ. In an isotropic and source-free region, the Maxwellian equations are given in the form of equations 1 and 2. Taking the curl of the equations and using the vector identity

$$\boldsymbol{\nabla} \times (\boldsymbol{\nabla} \times \ ) = \ \boldsymbol{\nabla} \ (\boldsymbol{\nabla} \cdot \ ) - \nabla^2, \qquad \text{(A-1)}$$

we see that both $\hat{\mathbf{E}}$ and $\hat{\mathbf{H}}$ satisfy the same wave equations,

$$\nabla^2\hat{\mathbf{E}} - \mu\varepsilon\partial_t^2\hat{\mathbf{E}} - \mu\sigma\partial_t\hat{\mathbf{E}} = 0 \qquad \text{(A-2)}$$

and

$$\nabla^2\hat{\mathbf{H}} - \mu\varepsilon\partial_t^2\hat{\mathbf{H}} - \mu\sigma\partial_t\hat{\mathbf{H}} = 0, \qquad \text{(A-3)}$$

which show that $\hat{\mathbf{E}}$ and $\hat{\mathbf{H}}$ must propagate as dissipative wave motion.

For EM waves that are simple-harmonic with time dependence $\exp(-i\omega t)$, the equations for the space dependence of $\mathbf{E}$ and $\mathbf{H}$ are Helmholtz equations given as

$$(\nabla^2 + k^2)\mathbf{E} = 0 \qquad \text{(A-4)}$$

and

$$(\nabla^2 + k^2)\mathbf{H} = 0, \qquad \text{(A-5)}$$

where

$$k^2 = \omega^2\mu\varepsilon\left(1 + \frac{i\sigma}{\omega\varepsilon}\right) \qquad \text{(A-6)}$$

is the squared wavenumber. The wavenumber, which characterizes the interaction between the EM field and the physical properties of the medium and frequency, can be written

$$k = \kappa_+ + i\kappa_-, \qquad \text{(A-7)}$$

where

$$\kappa_\pm = \omega\sqrt{\frac{\varepsilon\mu}{2}\left[\left(1 + \frac{\sigma^2}{\omega^2\varepsilon^2}\right)^{1/2} \pm 1\right]}. \qquad \text{(A-8)}$$

For the space dependency, the imaginary part of the wavenumber leads to the attenuation of a propagating EM wave in space. It is customary to write

$$k = \omega\sqrt{\widetilde{\varepsilon}\mu}, \qquad \text{(A-9)}$$

with now-complex permittivity $\widetilde{\varepsilon}$ defined by equation 12 to absorb the conductivity as its imaginary part.

For a unit impulse in direction n at $\mathbf{x}'$, the mth component of the EM Green's function is defined by the equation

$$(\partial_i\partial_i + k^2)G_{mn} = -i\omega\mu(\delta_{mn} + k^{-2}\partial_m\partial_n)\delta(\mathbf{x} - \mathbf{x}'), \qquad \text{(A-10)}$$

where Einstein's summation convention for the repeated-integer indices is used, and where δ_{mn} and $\delta(\mathbf{x})$ are the Kroenecker and Dirac delta functions, respectively. The EM Green's function, being a tensor, defines the impulse response of the medium. We consider a homogeneous medium. Introducing the scalar Green's function that is associated with the EM field, obeying $(\nabla^2 + k^2)g = -\delta(\mathbf{x} - \mathbf{x}')$, with the well-known form

$$g = \frac{1}{4\pi R}\exp(ikR), \qquad \text{(A-11)}$$

where $R = |\mathbf{x} - \mathbf{x}'|$, the solution for G_{mn} can be written

$$G_{mn}(\mathbf{x},\mathbf{0}) = i\omega\mu(\delta_{mn} + k^{-2}\partial_m\partial_n)g(R) \qquad \text{(A-12)}$$

or

$$G_{mn}(\mathbf{x},\mathbf{0}) = i\omega\mu\left\{\delta_{mn}[1 - (ikR)^{-1} + (ikR)^{-2}] + \frac{x_mx_n}{R^2}\right.$$
$$\left.\times\ [-1 + 3(ikR)^{-1} + 3(ikR)^{-2}]\right\}g(R).$$
$$\text{(A-13)}$$

In the following, to analyze the attenuation characteristics of the EM field, it is sufficient to consider the scalar Green's function.

For very high frequencies, $\omega \gg \sigma/\varepsilon$, the wavenumber is real and is given as

$$k \approx \omega\sqrt{\varepsilon\mu}, \qquad \text{(A-14)}$$

and its dependence on electric conductivity is negligible. Conduction currents are much smaller than displacement currents and can be neglected. The scalar Green's function becomes

$$g \approx \frac{1}{4\pi R}\exp(i\omega\sqrt{\varepsilon\mu}R). \qquad \text{(A-15)}$$

Under this circumstance, the EM field propagates as a wave without significant attenuation.

For very low frequencies, $\omega \ll \sigma/\varepsilon$, as in the EMSBL experiment, the behavior of the field is said to be diffusive. The squared wavenumber is purely imaginary,

$$k^2 \approx i\omega\mu\sigma, \tag{A-16}$$

and its dependence on electric permittivity is negligible. Displacement currents are much smaller than conduction currents and can be neglected. Formally, equations A-2–A-5 then represent diffusion equations. Setting $\sqrt{i} = (1 + i)/\sqrt{2}$, the wavenumber is written

$$k \approx (1 + i)\kappa, \tag{A-17}$$

with the real component

$$\kappa = \kappa_+ = \kappa_- = \sqrt{\frac{\omega\mu\sigma}{2}}. \tag{A-18}$$

Under this circumstance, the scalar Green's function that is associated with the EM field is

$$g = \frac{1}{4\pi R} \exp(i\kappa R)\exp(-\kappa R). \tag{A-19}$$

Because κ is real, the wave both varies sinusoidally and is attenuated with distance. In one wavelength, the attenuation of the field is $\exp(-2\pi) \approx 1.87 \times 10^{-3}$.

This appendix demonstrates that the EMSBL method can be based on the theory of EM-wave propagation in conductive media. Therefore, decomposition of EMSBL data into upgoing and downgoing fields can be based on EM-wave theory for conductive media. In particular, the EM-field decomposition need not be based on pure diffusion equations. We have shown that the EMSBL field's diffusion properties are embedded in its wave properties. Our description of field decomposition is valid for both conductive and nonconductive media. Low-frequency EMSBL recordings are handled by reducing the complex permittivity and the complex velocity according to equations 14 and 15. Nonconductive media are treated by letting $\sigma = 0$. In this case, the wavenumber is real, the velocity is independent of frequency, and the wave propagation is nondispersive, with no attenuation.

REFERENCES

Amundsen, H. E. F., S. Johansen, and T. Røsten, 2004, A seabed logging (SBL) calibration survey over the Troll gas field: Presented at the 66th Conference and Exhibition EAGE.

Amundsen, L., and A. Reitan, 1995, Decomposition of multicomponent seafloor data into upgoing and downgoing *P*- and *S*-waves: Geophysics, **60**, 563–572.

Berdichevsky, M. N., and M. S. Zhdanov, 1984, Advanced theory of deep geomagnetic sounding: Elsevier Science Publishing Company, Inc.

Chave, A. D., and C. S. Cox, 1982, Controlled electromagnetic sources for measuring electrical conductivity beneath the oceans. 1. Forward problem and model study: Journal of Geophysical Research, **87**, 5327–5338.

Eidesmo, T., S. Ellingsrud, L. M. MacGregor, S. Constable, M. C. Sinha, S. Johansen, F. N. Kong, and H. Westerdahl, 2002, Sea bed logging (SBL), a new method for remote and direct identification of hydrocarbon filled layers in deepwater areas: First Break, **20**, 144–152.

Ellingsrud, S., T. Eidesmo, S. Johansen, M. C. Sinha, L. M. MacGregor, and S. Constable, 2002, Remote sensing of hydrocarbon layers by seabed logging (SBL): Results from a cruise offshore Angola: The Leading Edge, **21**, 972–982.

Griffiths, D. J., 1999, Introduction to electrodynamics: Prentice Hall, Inc.

Ikelle, L. T., and L. Amundsen, 2005, Introduction to petroleum seismology: SEG.

Jackson, J. D., 1999, Classical electrodynamics, 3rd edition: John Wiley & Sons, Inc.

Kennett, B. L. N., 1983, Seismic wave propagation in stratified media: Cambridge Univ. Press.

Levy, S., D. Oldenburg, and J. Wang, 1988, Subsurface imaging using magnetotelluric data: Geophysics, **53**, 104–117.

Løseth, L., 2000, Electromagnetic waves in layered media: M.Sc. thesis, Norwegian University of Science and Technology.

Løseth, L., H. M. Pedersen, B. Ursin, L. Amundsen, and S. Ellingsrud, 2006, Low-frequency electromagnetic fields in applied geophysics: Waves or diffusion?: Geophysics, **71**, this issue.

Mittet, R., L. Løseth, and S. Ellingsrud, 2004, Inversion of SBL data acquired in shallow waters: Presented at the 66th Conference and Exhibition, EAGE.

Morse, P. M., and H. Feshbach, 1953, Methods of theoretical physics: McGraw-Hill Book Company.

Osborne, P., and S. Evans, 1987, Troll field: reservoir geology and field development planning, *in* J. Kleppe, E. W. Berg, T. E. Buller, O. Hjelmeland, and O. Torsaeter, eds., North Sea oil and gas reservoirs: The Norwegian Institute of Technology, 39–60.

Røsten, T., and L. Amundsen, 2004, Generalized electromagnetic seabed logging wavefield decomposition into *U/D*-going components: 74th Annual International Meeting, SEG, Expanded Abstracts, 592–595.

Sinha, M. C., P. D. Patel, M. J. Unsworth, T. R. E. Owen, and M. G. R. MacCormack, 1990, An active source electromagnetic sounding system for marine use: Marine Geophysical Researches, **12**, 59–68.

Ulaby, F. T., 2001, Fundamentals of applied electromagnetics: Prentice-Hall, Inc.

Ursin, B., 1983, Review of elastic and electromagnetic wave propagation in horizontally layered media: Geophysics, **48**, 1063–1081.

van der Kruk, J., 2001, Three-dimensional imaging of multi-component ground penetrating radar data: Ph.D. thesis, Delft University of Technology.

Vozoff, K., ed., 1986, Magnetotelluric methods: SEG.

Young, P. D., and C. S. Cox, 1981, Electromagnetic active source sounding near the East Pacific Rise: Geophysical Research Letters, **8**, 1043–1046.

Wait, J. R., 1970, Electromagnetic waves in stratified media: Pergamon Press Inc.

Ward, S. H., and G. W. Hohmann, 1987, Electromagnetic theory for geophysical applications, *in* M. N. Nabighian, ed., Electromagnetic methods in applied geophysics — Vol. 1, Theory: SEG.

Zhdanov, M. S., P. Traynin, and J. R. Booker, 1996, Underground imaging by frequency-domain electromagnetic migration: Geophysics, **61**, 666–682.